Influence of stretching and compression deformations on the electrical conductive properties of graphene-nanotube composites with an island-type topology

© *M.M. Slepchenkov, P.V. Barkov, O.E. Glukhova*

Saratov National Research State University,
Saratov, Russia
e-mail: slepchenkovm@mail.ru

Within the framework of the self–consistent–charge density functional tight-binding method, we study the features of the atomic structure and electrical conductive properties of a hybrid graphene-nanotube film with an island topology under uniaxial stretching and compression. The hybrid film is a composite structure formed by AB-stacked bilayer graphene and horizontally oriented chiral single-walled carbon nanotubes of 1.2 nm in diameter. The regularities of the deformation behavior of the investigated hybrid structure are revealed and the limits of its strength are established. It is shown how the electrical resistance and the current-voltage characteristic of the film change under stretching/compression deformations.

Introduction

Carbon nanotubes (CNTs) and graphene have been the most intensively studied and demanded representatives of the family of nanocarbon allotropes for several decades [1,2]. In recent years, the number of fundamental and applied scientific studies devoted to hybrid structures combining graphene and CNTs has increased significantly [3–9]. Graphene-nanotube hybrid structures are classified according to the characteristic features of their atomic structure. In particular, a distinction is made between hybrid structures with a high content of CNTs and hybrid structures with a high content of graphene [10]. In hybrid structures with a high content of CNTs, small sheets of graphene are attached to the outer walls of CNTs. Such configurations of graphene-nanotube hybrids can serve as an electrocatalyst for oxygen reduction [11]. Hybrid structures with a high content of graphene are divided into two classes: 1) hybrids in which CNTs are horizontally oriented with respect to graphene [12–14]; 2) hybrids in which CNTs are vertically oriented with respect to graphene [15–17]. Hybrid structures with horizontally oriented CNTs are a promising material for flexible electronics and all-carbon transistors [3], while hybrid structures with vertically oriented CNTs are promising for hydrogen storage, fabrication of supercapacitor electrodes, and as materials for thermal interface [15–17].

Hybrid structures with horizontally oriented CNTs are most widespread in practice. Taking into account the different types of chirality of CNTs and the different nature of the bond (covalent or via van der Waals forces) between graphene and CNTs in a hybrid, one can speak of a variety of topological configurations of hybrid graphene−CNT structures. In this regard, computer simulation studies are of particular value, which make it possible to predict which configurations of the hybrid structure are characterized by more favorable properties [18–23]. The most discussed issue in the scientific literature of recent years is quantum transport in graphene−CNT hybrid structures with horizontally oriented nanotubes. Both covalently bonded graphene−CNT structures [18,19] and those held by van der Waals forces [20,21] were considered. Regularities in the transport properties of graphene−CNT structures are revealed depending on the type of CNT conductivity [18], the distance between CNTs [19], the graphene-CNT distance [20], and the width and shape of the graphene nanoribbon edge [21].

At the same time, non-chiral single-walled carbon nanotubes (SWCNTs) were used in the papers noted above to construct topological models of graphene−CNT hybrid structures, while most synthesized SWCNTs are chiral tubes with a diameter of ∼ 1.2 nm [24]. In addition, when synthesizing graphene−CNT hybrids with horizontally oriented nanotubes, structures are often obtained with areas of increased density of carbon atoms, where CNT and graphene overlap each other [25,26]. In this regard, here we consider a hybrid graphene−nanotube structure with chiral SWCNTs (12,6) of subnanometer diameter and bilayer graphene, which form local „islands" with an increased carbon content. The purpose of this work is to study predictively the behavior of such a structure under the action of tensile/compressive deformation and to analyze changes in its electrical conductive properties.
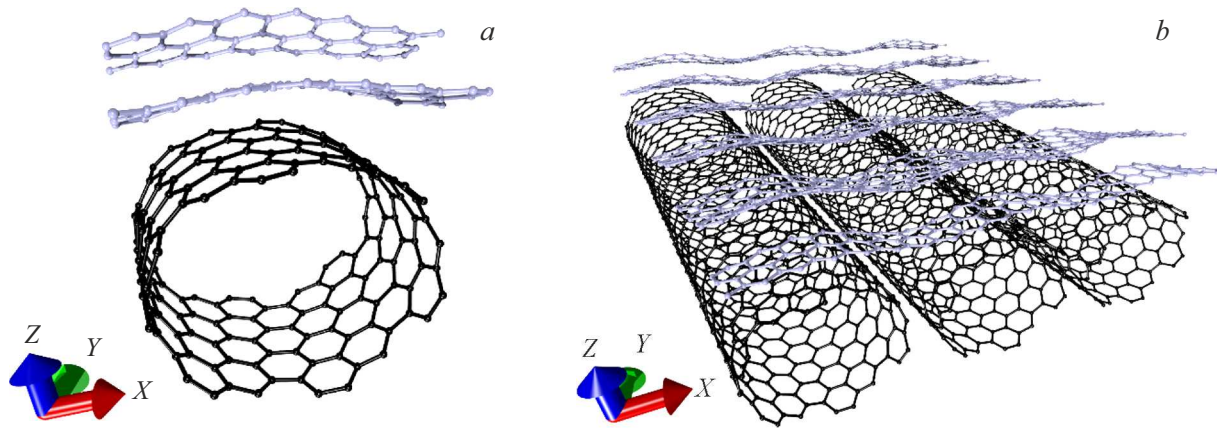
Figure 1. Atomic structure of the bilayer graphene−SWCNT (12,6) hybrid film with island topology: *a* — supercell; *b* — extended fragment.

1. Research methods

Calculations of the atomic configuration and energy parameters of the investigated graphene-nanotube hybrid structure were carried out within the framework of the self-consistent-charge density-functional tight-binding method (SCC-DFTB), implemented in the DFTB+ 20.2 [27] software package The SCC-DFTB model uses the valence approximation, according to which the largest contribution to the total energy of the system is made by valence orbitals described in terms of the basis of Slater-type orbitals with Slater−Koster parameters pbc-0-3 [27]. The tight binding approximation is incorporated into the DFT model using perturbation theory. The distribution of the electron charge density over atoms and, accordingly, the excess/deficient charge on atoms, is determined from the analysis of the populations according to the Mulliken scheme [28].

The static electrical conductivity G and current-voltage characteristic (CVC) of the structure under study were calculated in the framework of the Landauer−Buttiker formalism [29] using the formula

$$G = \frac{I}{V} = \frac{2e^2}{h} \int_{-\infty}^{\infty} T(E) F_T(E - E_F) dE, \qquad (1)$$

where $T(E)$ is the electron transmission function, F_T is the function describing thermal broadening of energy levels, E_F is the Fermi energy of the material of the electrodes to which the investigated object is connected, e is the electron charge, h is the Planck constant, $2e^2/h$ is the value of the conduction quantum doubled to take the spin into account. The electron transmission function $T(E)$ is expressed as

$$T(E) = \frac{1}{N} \sum_{k=1}^{N} \mathrm{Tr}\big(\Gamma_S(E) G_C^A(E) \Gamma_D(E) G_C^R(E)\big), \qquad (2)$$

where $G_C^A(E)$, $G_C^R(E)$ are the advanced and retarded Green's matrices describing the contact with electrodes, $\Gamma_S(E)$,

$\Gamma_D(E)$ are the energy level broadening matrices for the source and drain. All calculations were performed at a temperature of 300 K

2. Results and discussion

The studies were carried out for a supercell of a hybrid island-type graphene-nanotube film formed by a bilayer graphene zigzag nanoribbon with a width of 2 hexagons (0.5 nm) with the packing type of AB layers and SWCNTs with chirality indices (12,6). The bilayer graphene nanoribbon was located above the CNT perpendicular to its axis, forming the so-called „islands" of increased carbon density in the hybrid structure. Figure 1 shows the supercell of the bilayer graphene−SCWNT (12,6) hybrid film and its extended fragment obtained by multiple translation in two directions (along the X and Y axes). The shift between graphene layers along the Y axis (along the nanotube axis) was 0.48 nm, and the distance between them along the Z axis (perpendicular to the nanotube axis) was 0.34 nm. The translation vectors of the supercell along the X and Y axes are $L_x = 1.71$ nm and $L_y = 1.13$ nm. The thermodynamic stability of the constructed supercell was estimated from the enthalpy of formation, which was calculated according to the following formula:

$$\Delta H_f = (E_{\mathrm{film}} - E_{\mathrm{gr}} - E_{\mathrm{tube}})/N, \qquad (3)$$

where E_{film} is the energy of bilayer graphene−SWCNT (12,6) hybrid film, E_{gr} is the energy of bilayer graphene, E_{tube} is the nanotube (12,6) energy, N is the number of atoms in the supercell. The atomic structure of the supercell of the hybrid graphene-nanotube film was configured make its total energy absolute value be less than the energy of its individual components. The calculated value of ΔH_f was -0.17 eV/at, therefore, the considered supercell atomic configuration is energetically stable.

Let us proceed to the study of the effect of axial stretching/compression deformation on the atomic structure
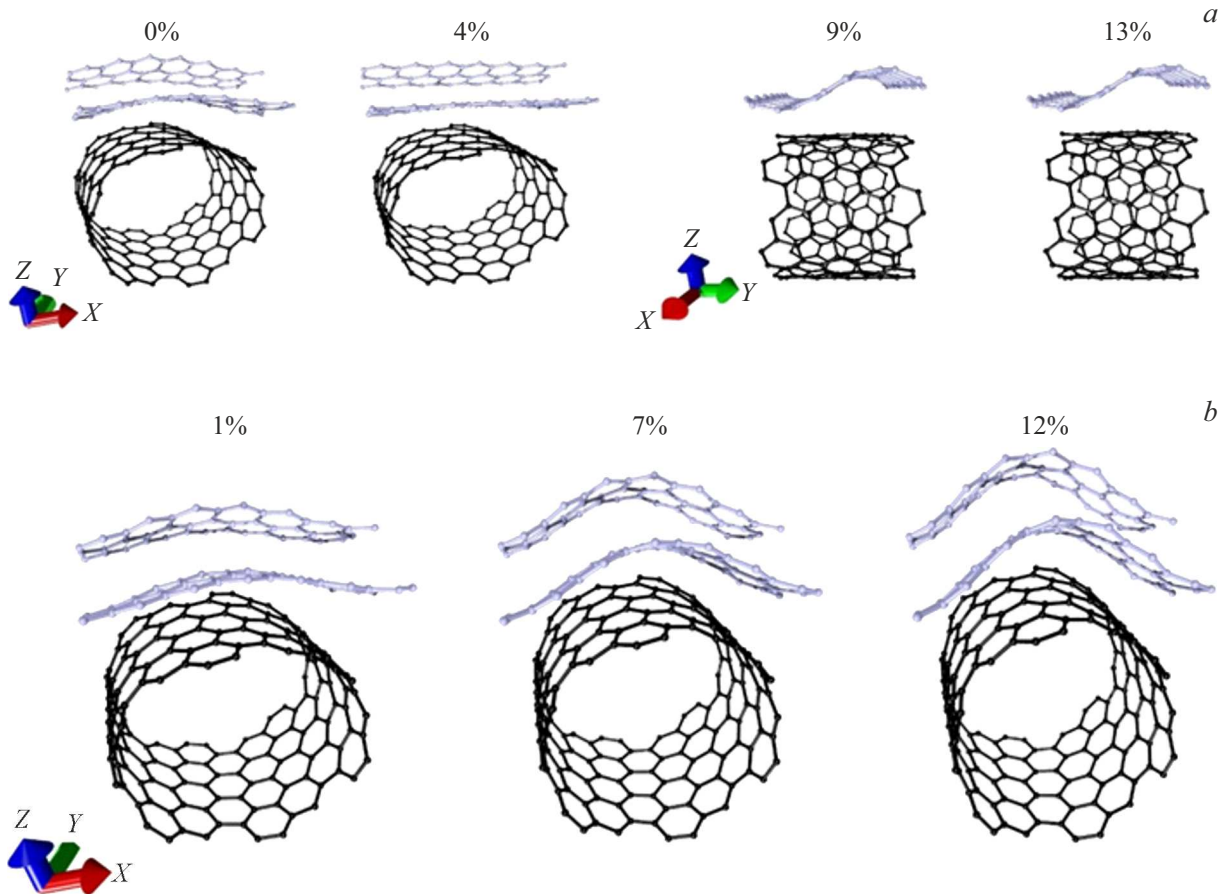
Figure 2. Changes in the atomic structure of the hybrid film bilayer graphene−SWCNT (12,6) upon deformation along the X axis: a — stretching; b — compression.

and electrical conductive properties of the studied graphene-nanotube film. In the course of the numerical experiments, we considered the stretching/compression of the supercell along the X axis, i. e., along the zigzag direction of the bilayer graphene. This option of applying deformation is due to two reasons: 1) bilayer graphene and nanotube (12,6) in the composition of the supercell of the hybrid structure are not bound by covalent bonds, but interact through van der Waals forces; 2) bilayer graphene in the composition of a supercell has the shape of a nanoribbon. At each deformation step, the length of the translation vector L_x of the supercell changed by 1% (increased in the case of stretching and decreased in the case of compression). Then, the atomic structure of the supercell was optimized by minimizing its total energy over the coordinates of all atoms. Figure 2 demonstrates the changes in the atomic structure of the bilayer graphene−SWCNT (12,6) hybrid film with an increase in tensile (Fig. 2, a) and compression strain (Fig. 2, b). It can be seen from Fig. 2, a that as the film is stretched, the graphene bilayer first tends to straighten, and when it is stretched by 9%, its atomic network transforms from flat to wavy with two half-waves, i.e. the transition of the structure to a new phase state occurs. Such changes can be explained by the small width of

the graphene nanoribbon comprised in the supercell, as well as by the fact that, at such a deformation value, the distance between the deformed graphene layers along the Y axis becomes sufficient for the formation of covalent bonds. With compression, as can be seen from Fig. 2, b, the graphene bilayer takes the form of an arc with a uniformly increasing amplitude at each deformation step, and the nanotube takes the form of an prolate ellipsoid. In this case, the structure under study demonstrates almost the same ultimate strength in both cases of deformation: the destruction of the covalent bonds of the atomic network occurs at stretching by 14% and at compression by 13%.

Figure 3 shows the plots of the change in the deformation energy of stretching E_{str} (Fig. 3, a) and compression E_{com} (Fig. 3, b) as the length of the translation vector ΔL of the supercell of the hybrid film changes along the X axis (in relative units). The deformation energy was calculated as the difference between the total energy of the structure before and after stretching/compression divided by the number of atoms in the supercell. It can be seen from the plot in Fig. 3, a that, up to the case of stretching by 8%, the function $E_{str}(\Delta L)$ increases according to a quadratic law, which is characteristic of elastic deformation. When the structure is stretched by 9% or more, the quadratic
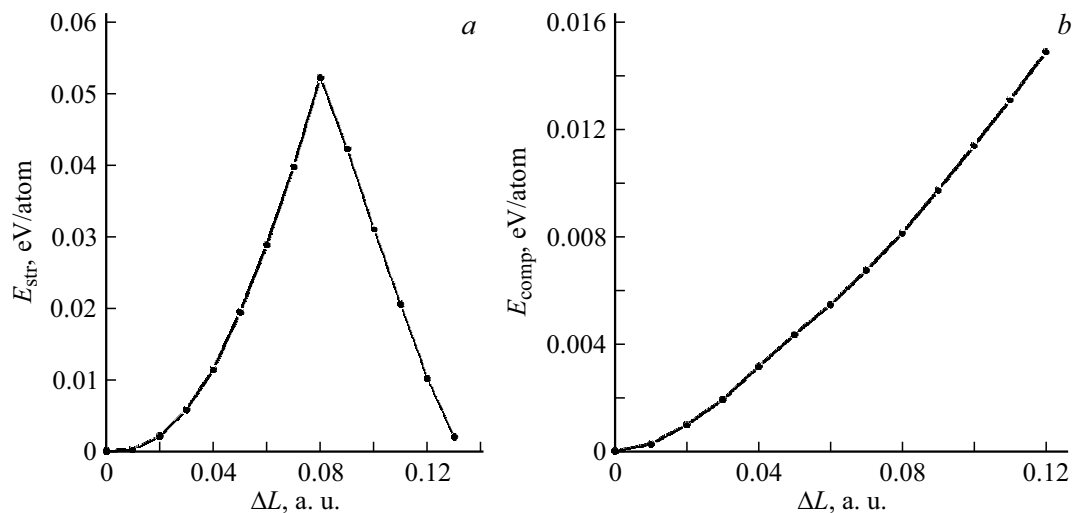
Figure 3. Plots of the deformation energy of the bilayer graphene−SWCNT (12,6) hybrid film under stretching (*a*) and compression (*b*). The value of deformation along the *X* axis is given in relative units of ΔL.
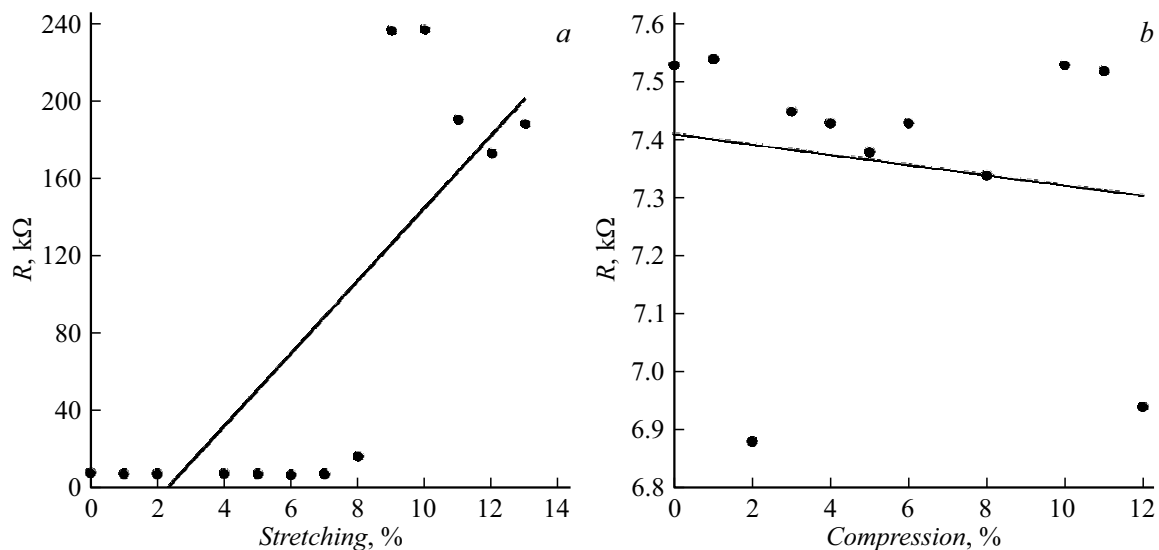
Figure 4. Change in the electrical resistance of a bilayer graphene−SWCNT (12,6) hybrid film with an island topology under axial deformation: *a* — stretching; *b* — compression.

increase in $E_{str}(\Delta L)$ is replaced by a decrease, which indicates the transition from elastic to plastic deformation. This explains the transformation of the atomic structure of the hybrid graphene-nanotube film from flat to wavy described above. The dependence $E_{com}(\Delta L)$ presented in Fig. 3, *b* demonstrates a nearly quadratic increase in the deformation energy with compression, which indicates an elastic deformation of the graphene−SWCNT (12,6) hybrid film in this case.

To assess the effect of axial deformation on the electrical conductive properties of a bilayer graphene−SWCNT (12,6) hybrid film, the electrical resistance and CVCs were calculated. The plots in Fig. 4 show how the resistance of the film changes as it is stretched (Fig. 4, *a*) and compressed (Fig. 4, *b*). From Fig. 4, *a* it can be seen that the

transformation of the flat structure of the graphene bilayer into a wave-like structure upon stretching by 9% causes an increase in the resistance of the film by a factor of 40 ($\sim 236\,k\Omega$) compared with the value in the absence of deformation ($\sim 7.5\,k\Omega$). In the stretching interval 1−7%, the resistance value changes little ($\sim 6.8- \sim 7.2\,k\Omega$) compared to the initial value for the undeformed structure. The resistance behaves quite stably under axial compression. From the plot in Fig. 4, *b*, one can see that in the studied interval of deformations, the resistance value changes in the range $\sim 7.5- \sim 6.9\,k\Omega$. The revealed features of the electrical resistance behavior in the hybrid film under axial stretching/compression are explained by the laws of the change in the Fermi level in each of the considered cases of deformation. When stretched by 1−7%, the Fermi
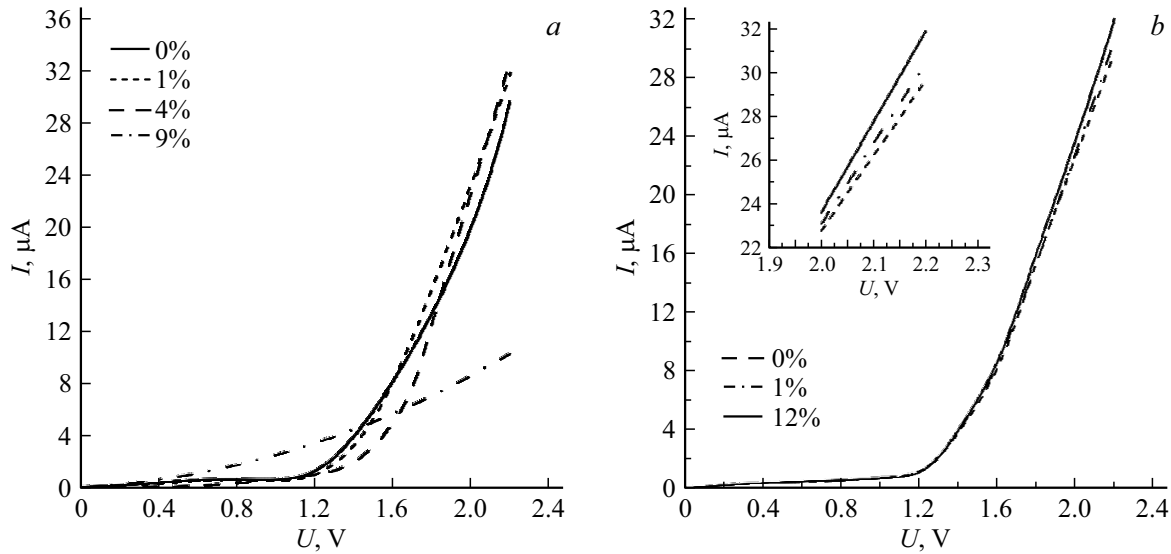
Figure 5. CVC of a bilayer graphene−SWCNT (12,6) hybrid film with an island topology for various cases of axial deformations: *a* — stretching; *b* — compression.

level of the film changes insignificantly within the limits $(-4.97 - -4.90 \text{ eV})$, whereas after the transformation of the atomic network of the graphene bilayer from flat to wavy, the Fermi level immediately shifts up the energy axis by 0.2 eV, which testifies for a rearrangement of the electronic structure of the material. In particular, upon stretching by 9%, an energy gap of 0.004 eV appears in the band structure of the hybrid film. The steady position of the Fermi level of the hybrid film (-4.70 eV) is close to the Fermi level of an ordinary graphene sheet (-4.67 eV). The calculated resistance of the wavy graphene bilayer is $\sim 236 \text{ k}\Omega$, which confirms the determining influence of the graphene bilayer on the electrical conductive properties of the bilayer graphene−SWNT (12,6) hybrid film. Under compression, the Fermi level of the hybrid film practically does not change, remaining within $-4.88 - -4.87 \text{ eV}$. There is no energy gap between the valence band and the conduction band in this case, as well as for the undeformed structure of the bilayer graphene−SWCNT (12,6) hybrid film.

Figure 5 shows the calculated current-voltage characteristics under stretching (Fig. 5, *a*) and compression (Fig. 5, *b*) of the bilayer graphene−SWCNT (12,6) hybrid film by various percentages. The revealed patterns of changes in the atomic structure of the film under axial stretching/compression are also reflected in the behavior of the CVC. Figure 5, *a* clearly demonstrates that, when stretched by 1 and 4%, the slope of the I−V characteristic and the maximum current value at a voltage of 2.2 V change little compared to the values for an undeformed film, as was found above and for resistance. During the transition of the hybrid film to a new phase state with a wave-like atomic network of the graphene bilayer (stretching by 9%), both the slope of the CVCs and the current maximum decrease

(approximately by a factor of 4). On the contrary, a uniform increase in the arc amplitude of the graphene bilayer during compression and slight changes in the resistance in this case lead to a stable behavior of the CVC in Fig. 5, *b*. On the whole, it can be noted that the electrical conductive properties of the investigated bilayer graphene−SWCNT (12,6) hybrid film with an island topology are insensitive to axial compression.

Conclusion

Thus, for the first time, we have studied the deformation behavior of bilayer graphene−SWCNT (12,6) hybrid films with an island topology under axial stretching/compression and revealed the regularities in the behavior of their electrical conductive properties affected by both types of deformation. It is shown that in the case of axial stretching by 9%, the hybrid film undergoes a transition to a new phase state with a wavy structure of the graphene bilayer. This transition is accompanied by the appearance of an energy gap in the electronic structure, an increase in the resistance by a factor of ten, and a decrease in the slope of the CVCs by several times. Under axial compression, the resistance and current values change little compared to the values for the undeformed film, in terms of values of current, hybrid films of bilayer graphene−SWCNT (12,6) outperform various structural modifications of graphene, in particular, hybrid films based on graphene and organic molecules by 2 orders of magnitude [30] and graphene nanoribbons by 3 orders [31]. Based on the obtained results, it can be predicted that such graphene-nanotube films with island topology can be promising for further application in flexible and extensible electronic devices, in particular, as conducting electrodes.

Funding

Conflict of interest

The authors declare that they have no conflict of interest.

References

[1] S. Rathinavel, K. Priyadharshini, D. Panda. Mater. Sci. Eng. B, **268**, 115095 (2021). DOI: 10.1016/j.mseb.2021.115095

[2] F. Zhang, K. Yang, G. Liu, Y. Chen, M. Wang, S. Li, R. Li. Compos. Part A Appl. Sci. Manuf., **160**, 107051 (2022). DOI: 10.1016/j.compositesa.2022.107051

[3] B. Cai, H. Yin, T. Huo, J. Ma, Z. Di, M. Li, N. Hu, Z. Yang, Y. Zhang, Y. Su. J. Mater. Chem. C, **8** (10), 3386 (2020). DOI: 10.1039/C9TC06586E

[4] Y. Han, Y. Jiang, C. Gao, ACS Appl. Mater. Interfaces, **7** (15), 8147 (2015). DOI: 10.1021/acsami.5b00986

[5] Y. Li, Q. Ai, L. Mao, J. Guo, T. Gong, Y. Lin, G. Wu, W. Huang, X. Zhang. Sci. Rep., **11**, 21006 (2021). DOI: 10.1038/s41598-021-00307-5

[6] W. Du, Z. Ahmed, Q. Wang, C. Yu, Z. Feng, G. Li, M. Zhang, C. Zhou, R. Senegor, C.Y. Yang. 2D Mater., **6** (4), 042005 (2019). DOI: 10.1088/2053-1583/ab41d3

[7] S. Lepak-Kuc, K.Z. Milowska, S. Boncel, M. Szybowicz, A. Dychalska, I. Jozwik, K.K. Koziol, M. Jakubowska, A. Lekawa-Raus. ACS Appl. Mater. Interfaces, **11** (36), 33207 (2019). DOI: 10.1021/acsami.9b08198

[8] H. Kim, J. Kim, H.S. Jeong, H. Kim, H. Lee, J.M. Ha, S.M. Choi, T.H. Kim, Y.C. Nah, T.J. Shin, J. Bang, S.K. Satijag, J. Koo. Chem. Commun., **54** (41), 5229 (2018). DOI: 10.1039/C8CC02148A

[9] K. Yousefi, J. Environ. Treat. Tech., **9** (1), 224 (2021). DOI: 10.47277/JETT/9(1)232

[10] R.T. Lv, E. Cruz-Silva, M. Terrones. ACS Nano, **8** (5), 4061 (2014). DOI: 10.1021/nn502426c

[11] J. Zhou, Y. Zheng, D. Chen. Nanomaterials, **12** (4), 620 (2022). DOI: 10.3390/nano12040620

[12] L. Cai, X. Xue, M. Liu, H. Li, X. Zhou, G. Yu. APL Mater., **9** (4), 041110 (2021). DOI: 10.1063/5.0045100

[13] B. Abreu, M. Rocha, M. Nunes, C. Freire, E.F. Marques. J. Mater. Sci., **56**, 19512 (2021). DOI: 10.1007/s10853-021-06463-3

[14] T. Xu, D. Yang, Z. Fan, X. Li, Y. Liu, C. Guo, M. Zhang, Z.-Z. Yu. Carbon, **152** (134) (2019). DOI: 10.1016/j.carbon.2019.06.005

[15] A. Abdollahi, A. Abnavi, S. Ghasemi, S. Mohajerzadeh, Z. Sanaee. Electrochim. Acta, **320**, 134598 (2019). DOI: 10.1016/j.electacta.2019.134598

[16] Y. Li, Z. Li, L. Lei, T. Lan, Y. Li, P. Li, X. Lin, R. Liu, Z. Huang, X. Fen, Y. Ma. Flat. Chem., **15**, 100091 (2019). DOI: 10.1016/j.flatc.2019.100091

[17] Y. Zhou, W. Qian, W. Huang, B. Liu, H. Lin, C. Dong. Nanomaterials, **9** (10), 1450 (2019). DOI: 10.3390/nano9101450

[18] B.Yu. Valeev, A.N. Toksumakov, D.G. Kvashnin, L.A. Chernozatonskii. JETP Lett., **115** (2), 93 (2022). DOI: 10.1134/S0021364022020114

[19] O.E. Glukhova, M.M. Slepchenkov, V.V. Mitrofanov, P.V. Barkov, Semiconductors, **53** (12), 1677 (2019). DOI: 10.1134/S1063782619160097

[20] J. Srivastava, A. Gaur. J. Chem. Phys., **155** (24), 244104 (2021). DOI: 10.1063/5.0077099

[21] A.B. Felix, M. Pacheco, P. Orellana, A. Latgé. Nanomaterials, **12** (19), 3475 (2022). DOI: 10.3390/nano12193475

[22] J. Srivastava, A. Gaur. Nanoscale Adv., **3** (7), 2030 (2021). DOI: 10.1039/D0NA00881H

[23] E.F. Sheka, L.A. Chernozatonskii. J. Comput. Theor. Nanosci., **7** (9), 1814 (2010). DOI: 10.1166/jctn.2010.1546.

[24] S. Zhang, L. Tong, J. Zhang. Natl. Sci. Rev., **5** (3), 310 (2018). DOI: 10.1093/nsr/nwx080

[25] E. Zhou, J. Xi, Y. Guo, Y. Liu, Z. Xu, L. Peng, W. Gao, J. Ying, Z. Chen, C. Gao. Carbon, **133**, 316 (2018). DOI: 10.1016/j.carbon.2018.03.023

[26] J. Kuang, Z. Dai, L. Liu, Z. Yang, M. Jin, Z. Zhang. Nanoscale, **7** (20), 9252 (2015). DOI: 10.1039/C5NR00841G

[27] B. Hourahine, B. Aradi, V. Blum, F. Bonafé, A. Buccheri, C. Camacho, C. Cevallos, M.Y. Deshaye, T. Dumitrică, A. Dominguez, S. Ehlert, M. Elstner, T. van der Heide, J. Hermann, S. Irle, J.J. Kranz, C. Köhler, T. Kowalczyk, T. Kubař, I.S. Lee, V. Lutsker, R.J. Maurer, S.K. Min, I. Mitchell, C. Negre, T.A. Niehaus, A.M.N. Niklasson, A.J. Page, A. Pecchia, G. Penazzi, M.P. Persson, J. Řezáč, C.G. Sanchez, M. Sternberg, M. Stöhr, F. Stuckenberg, A. Tkatchenko, V.W.Z. Yu, T. Frauenheim. J. Chem. Phys., **152** (12), 124101 (2020). DOI: 10.1063/1.5143190

[28] R.S. Mulliken. J. Chem. Phys., **23**, 1833 (1955). DOI: 10.1063/1.1740588

[29] S. Datta. *Quantum Transport: Atom to Transistor* (Cambridge University Press, NY., 2005), p. 285−308.

[30] J. Liu, Q. Liang, R. Zhao, S. Lei, W. Hu. Mater. Chem. Front., **4** (2), 354 (2020). DOI: 10.1039/C9QM00517J

[31] O. Braun, J. Overbeck, M.E. Abbassi, S. Kaser, R. Furrer, A. Olziersky, A. Flasby, G.B. Barin, R. Darawish, K. Mullen, P. Ruffieux, R. Fasel, I. Shorubalko, M.L. Perrin, M. Calame. Carbon, **184**, 331 (2021). DOI: 10.1016/j.carbon.2021.08.001

Translated by Ego Translating